

# Displaced Vertex and Disappearing Track Signatures in type-III Seesaw

Sudip Jana<sup>1</sup>, Nobuchika Okada<sup>2</sup>, and Digesh Raut<sup>3</sup>

<sup>1</sup>*Max-Planck-Institut für Kernphysik,  
Saupfercheckweg 1, 69117 Heidelberg, Germany*

<sup>2</sup>*Department of Physics and Astronomy,  
University of Alabama, Tuscaloosa, Alabama 35487, USA*

<sup>3</sup>*Bartol Research Institute, Department of Physics and Astronomy,  
University of Delaware, Newark DE 19716, USA*

## Abstract

We investigate the prospect of probing the type III seesaw neutrino mass generation mechanism at various collider experiments by searching for a disappearing track signature as well as a displaced vertex originating from the decay of  $SU(2)_L$  triplet fermion ( $\Sigma$ ). Because the triplet fermion is primarily produced at colliders through the electroweak gauge interactions, its production rate is uniquely determined by its mass. Using the type III seesaw formula, we find that a  $\Sigma$  particle with mass of a few hundred GeV, once produced, leads to a disappearing track signature which can be probed at the LHC and high luminosity LHC while the displaced vertex signature can be probed by various proposed experiments such as MATHUSLA, LHeC, and FCC-he.

---

<sup>1</sup>sudip.jana@mpi-hd.mpg.de

<sup>2</sup>okadan@ua.edu

<sup>3</sup>draut@udel.edu

# 1 Introduction

The Standard Model (SM) of particle physics is a tremendously successful theory but it is incomplete in its current form. Among its various shortcomings, we here focus on the fact that the SM offers no explanation about the origin of the tiny masses of neutrinos [1]. One of the most appealing scenario to naturally generate the tiny neutrino masses is the well-known seesaw mechanism, namely, type-I seesaw [2,3], type-II seesaw [4] and type-III seesaw [5], which effectively generates the lepton number violating dimension five operator  $\mathcal{O}_5 = \frac{c}{\Lambda} LLHH$  at low energies, where  $\Lambda$  is the seesaw scale.

We concentrate on type-III seesaw, where in addition to the SM particles, at least two  $SU(2)_L$  triplet fermions ( $\Sigma$ ) with zero hypercharge are introduced [5]. The observed neutrino mass is then given by  $m_\nu \simeq Y_\nu^2 v^2 / M_\Sigma$ , where  $v$  is the electroweak vacuum expectation value (VEV),  $M_\Sigma$  is the triplet fermion mass, and  $Y_\nu$  is the Dirac Yukawa coupling. For example, if the type-III seesaw mechanism is incorporated in a grand unified theories (GUT) framework,  $M_\Sigma$  are of the intermediate scale [5–8]<sup>4</sup>. However, type-III seesaw scenario with  $M_\Sigma \simeq \mathcal{O}(1)$  TeV is also technically natural. Unlike GUT scenarios, the latter can be explored at collider experiments. See, for example Ref. [44]. Furthermore, we already have a dedicated search for the type-III scenario by the CMS [11] and the ATLAS collaborations [12] for the Large Hadron Collider (LHC). Particularly, their search focuses on prompt decay of neutral ( $\Sigma^0$ ) and charged ( $\Sigma^\pm$ ) components of  $\Sigma$  produced via an intermediate electroweak gauge boson, which yields two final-state leptons (electrons or muons) of different flavors and charge combinations accompanied by at least two jets. Assuming flavor-universal branching fractions of  $\Sigma^{0,\pm}$  into different lepton flavors,  $M_\Sigma < 840$  GeV is excluded [11]. The direct search for prompt decay of  $\Sigma^{0,\pm}$  with mass in a TeV range is very challenging at the LHC. The LHC can also search for the so-called disappearing track signature signal from  $\Sigma^\pm$  decay [13].

In this paper, we explore an interesting possibility that  $\Sigma^{0,\pm}$  can be long-lived and evade the prompt decay searches at the LHC, thereby explaining the null results from the LHC experiments. However, the vertex corresponding to the long-lived particle decay is displaced from the vertex where it was produced. This so-called displaced vertex event is very clean with almost zero SM events as background. The current status of the displaced vertex searches at the LHC can be found in Refs. [14–30]. We expect dramatic improvement of the search for the displaced vertex at future collider experiments, such as the proposed MAssive Timing Hodoscope for Ultra Stable neutraL pArticles (MATHUSLA) detector [31] for the high luminosity (HL)-LHC, the Large Hadron electron Collider (LHeC) [32], and the Future Circular electron-hadron Colliders (FCC-he) [33]. In the following, we show that the displaced vertex signature arising from the decay of  $\Sigma^{\pm,0}$  in type-III<sup>56</sup> seesaw can be probed at MATHUSLA, LHeC, and FCC-he experiments.

This work is organized as follows: In Sec. 2, we introduce the type-III seesaw mechanism and discuss the neutrino mass generation mechanism. In Sec. 3, we study the production of  $\Sigma^{\pm,0}$  at HL-LHC, LHeC, and FCC-he, and also estimate their decay lengths. After discussing the bounds from disappearing track search experiments as well its future prospect, in Sec. 4, we

---

<sup>4</sup>For a discussion of GUT scenario with  $M_\Sigma \lesssim \mathcal{O}(1)$  TeV, see Ref. [9].

<sup>5</sup>Such a prospect for type-I seesaw scenario at MATHUSLA experiment has been investigated in Refs [34,35].

<sup>6</sup>The prospect for type-II seesaw at HL-LHC and  $e^+ e^-$  collider was investigated in [36].

examine the prospect of observing the displaced vertex signal from  $\Sigma^{\pm,0}$  decay at MATHUSLA, LHeC, and FCC-he. Finally, we present our conclusion in Sec. 5.

## 2 The Type-III Seesaw

We consider the extension of the SM with three generation of  $SU(2)_L$  triplet fermions,  $\Sigma_i$  ( $i = 1, 2, 3$ ), and their Lagrangian is given by

$$\mathcal{L}_\Sigma = \text{Tr} [\bar{\Sigma}_i \not{D} \Sigma_i] - \left( \frac{1}{2} M_\Sigma^{ij} \text{Tr} [\bar{\Sigma}_i^c \Sigma_j] + \text{h.c.} \right) - \left( \sqrt{2} Y_\Sigma^{ij} \bar{L}_i \Sigma_j H + \text{h.c.} \right), \quad (2.1)$$

where  $D$  is the covariant derivative for  $\Sigma_i$ ,  $M_\Sigma = m_\Sigma \text{diag}(1, 1, 1)$  is the triplet fermions mass matrix assuming a degenerate mass spectrum for simplicity,  $Y_\Sigma^{ij}$  are the Yukawa couplings,  $L \equiv (\nu, l)^T$  is the left-handed SM lepton doublet,  $H \equiv (H^0, H^-)^T = ((v + h + i\eta)/\sqrt{2}, H^-)^T$  and  $v = 246$  GeV. The  $SU(2)_L$  triplet fermion can be expressed in terms of its charged ( $\Sigma^\pm$ ) and charge neutral component ( $\Sigma^0$ ) as

$$\Sigma = \begin{pmatrix} \Sigma^0/\sqrt{2} & \Sigma^+ \\ \Sigma^- & -\Sigma^0/\sqrt{2} \end{pmatrix}, \quad (2.2)$$

and its conjugate is given by  $\Sigma^c \equiv C\bar{\Sigma}^T$ , where  $C$  denotes the charge conjugation operator.

Let us first consider the masses of the charged ( $\Sigma^\pm$ ) and charge neutral ( $\Sigma^0$ ) component  $\Sigma^{0,\pm}$  of each triplet fermion. Although their masses are degenerate at the tree-level, radiative corrections induced by the electroweak gauge boson loops removes the degeneracy and generate mass-splitting between them. The resulting mass difference ( $\Delta M$ ) is given by [37]

$$\Delta M = \frac{\alpha_2 m_\Sigma}{4\pi} \left[ f \left( \frac{M_W}{m_\Sigma} \right) - \cos^2 \theta_W f \left( \frac{M_Z}{m_\Sigma} \right) \right]. \quad (2.3)$$

Here,  $\alpha_2 = 0.034$ ,  $\cos^2 \theta_W \simeq 0.769$  [40], and the function  $f$  is defined as

$$f(r) = r \left[ 2r^3 \ln r - 2r + (r^2 - 4)^{1/2} (r^2 + 2) \ln A \right] / 2, \quad (2.4)$$

where  $A = (r^2 - 2 - r\sqrt{r^2 - 4})/2$ . We show  $\Delta M$  as a function of  $m_\Sigma$  in Fig. 1. The dashed line denotes the  $\pi$  meson mass of 140 MeV.

The Yukawa coupling between  $H$  and  $\Sigma$  generates a mass-mixing term between  $\Sigma^{0,\pm}$ ,  $\nu_\ell$ , and  $\ell_L$ . The mixing mass matrix involving the charged fermion states ( $M_\pm$ ) and neutral fermion states ( $M_0$ ) in the  $(l^\pm, \Sigma^\pm)$  and  $(\nu, \Sigma^0)$  basis, respectively, are expressed as

$$M_\pm = \begin{pmatrix} m_{\ell^\pm} & \sqrt{2} m_D \\ 0 & M_\Sigma \end{pmatrix}, \quad M_0 = \begin{pmatrix} 0 & m_D \\ m_D^T & M_\Sigma \end{pmatrix}, \quad (2.5)$$

where  $m_{\ell^\pm}$  and  $m_D^{ij} = Y_\Sigma^{ij} v/\sqrt{2}$  are the Dirac type mass for the SM charged leptons and  $\Sigma$ , respectively. It shows that the mixings between heavy triplet and light SM states in both the neutral and charged fermion sectors are of the order  $m_D M_\Sigma^{-1}$ . We here focus on the mixing in

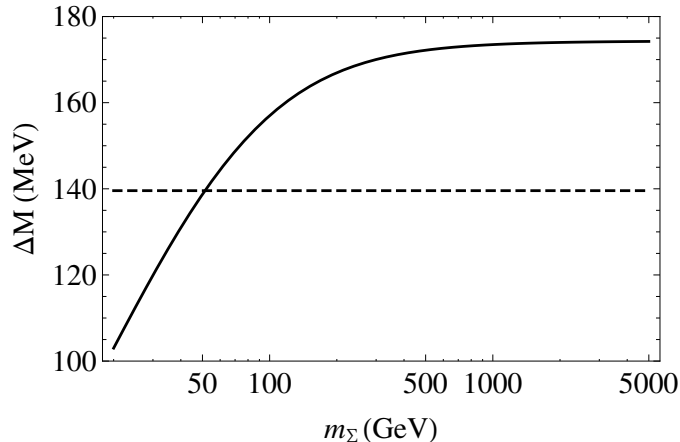


Figure 1: The mass-splitting between  $\Sigma^\pm$  and  $\Sigma^0$  induced by radiative corrections as a function of  $m_\Sigma$ . Dashed line denotes the  $\pi$  meson mass.

the neutral sector which generates the observed neutrino masses. The Feynman diagram for the type-III seesaw is shown in Fig. 2. The light neutrino mass matrix is generated as

$$m_\nu \simeq m_D (M_\Sigma)^{-1} m_D^T. \quad (2.6)$$

We can express the neutrino flavor eigenstate ( $\nu$ ) as  $\nu \simeq \mathcal{N}\nu_m + \mathcal{R}N_m$ , where  $\nu_m$  ( $\Sigma_m$ ) are light (heavy) mass eigenstates,  $\mathcal{R} = m_D(M_\Sigma)^{-1}$ ,  $\mathcal{N} = \left(1 - \frac{1}{2}\mathcal{R}^*\mathcal{R}^T\right)U_{\text{MNS}} \simeq U_{\text{MNS}}$ . The neutrinos mass mixing matrix  $U_{\text{MNS}}$  diagonalizes the light neutrino mass matrix as follows:

$$U_{\text{MNS}}^T m_\nu U_{\text{MNS}} = D_\nu = \text{diag}(m_1, m_2, m_3), \quad (2.7)$$

where

$$U_{\text{MNS}} = \begin{pmatrix} c_{12}c_{13} & c_{12}c_{13} & s_{13}e^{-i\delta} \\ -s_{12}c_{23} - c_{12}s_{23}s_{13}e^{i\delta} & c_{12}c_{23} - s_{12}s_{23}s_{13}e^{i\delta} & s_{23}c_{13} \\ s_{12}c_{23} - c_{12}c_{23}s_{13}e^{i\delta} & -c_{12}s_{23} - s_{12}c_{23}s_{13}e^{i\delta} & c_{23}c_{13} \end{pmatrix} \begin{pmatrix} 1 & 0 & 0 \\ 0 & e^{-i\rho_1} & 0 \\ 0 & 0 & e^{-i\rho_2} \end{pmatrix}. \quad (2.8)$$

Here,  $c_{ij} = \cos \theta_{ij}$ ,  $s_{ij} = \sin \theta_{ij}$ , we set the Majorana phases  $\rho_{1,2} = 0$  for simplicity, and set Dirac  $CP$ -phase  $\delta = \frac{3\pi}{2}$  [38]. The rest of the parameters are fixed to reproduce the neutrino oscillation data, for which we adopt  $\sin^2 2\theta_{13} = 0.092$  [39] along with  $\sin^2 2\theta_{12} = 0.87$ ,  $\sin^2 2\theta_{23} = 1.0$ ,  $\Delta m_{12}^2 = m_2^2 - m_1^2 = 7.6 \times 10^{-5} \text{ eV}^2$ , and  $\Delta m_{23}^2 = |m_3^2 - m_2^2| = 2.4 \times 10^{-3} \text{ eV}^2$  [40] with three neutrino mass eigenvalues  $m_{1,2,3}$ .

From Eqs. (2.6) and (2.7), the Dirac mass matrix can be parameterized as [41]

$$m_D = U_{\text{MNS}}^* \sqrt{D_\nu} O \sqrt{M_\Sigma} = \frac{1}{m_\Sigma} U_{\text{MNS}}^* \sqrt{D_\nu} O, \quad (2.9)$$

where  $\sqrt{D_\nu} = \text{diag}(\sqrt{m_1}, \sqrt{m_2}, \sqrt{m_3})$ ,  $O$  is a general orthogonal matrix, and we have used  $\sqrt{M_\Sigma} = \sqrt{m_\Sigma} \text{diag}(1, 1, 1)$  to obtain the last expression. We parameterize the general orthog-

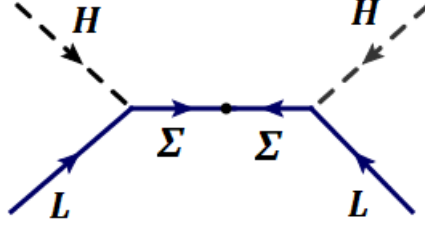


Figure 2: Tree-level neutrino mass diagram for Type-III seesaw mechanism.

onal matrix  $O$  as

$$O = \begin{pmatrix} 1 & 0 & 0 \\ 0 & \cos \theta_1 & \sin \theta_1 \\ 0 & -\sin \theta_1 & \cos \theta_1 \end{pmatrix} \begin{pmatrix} \cos \theta_2 & 0 & \sin \theta_2 \\ 0 & 1 & 0 \\ -\sin \theta_2 & 0 & \cos \theta_2 \end{pmatrix} \begin{pmatrix} \cos \theta_3 & \sin \theta_3 & 0 \\ -\sin \theta_3 & \cos \theta_3 & 0 \\ 0 & 0 & 1 \end{pmatrix}, \quad (2.10)$$

where the  $\theta_1$ ,  $\theta_2$ , and  $\theta_3$  are complex numbers.

In the rest of the analysis, for the observed neutrino mass spectrum, we consider both the normal hierarchy (NH),  $m_1 < m_2 < m_3$ , and the inverted hierarchy (IH),  $m_3 < m_1 < m_2$ . Note that the observed light neutrino mass spectrum is uniquely determined once we fix the lightest neutrino mass:  $m_1$  ( $m_3$ ) for the NH (IH).

### 3 Production and Decay Modes of Fermion Triplets

Let us discuss the the production of  $\Sigma^{0,\pm}$  at various collider experiments. Because  $\Sigma$  is a  $SU(2)_L$  triplet, the distinctive feature of the type III seesaw scenario is that  $\Sigma^{0,\pm}$  can be produced at colliders directly through their electroweak gauge interactions. At the LHC, the singly charged ( $\Sigma^\pm$ ) are pair-produced from  $q\bar{q}$  fusion through  $s$ -channel  $Z/\gamma$  exchange as shown in the left diagram of Fig. 3. Similarly,  $s$ -channel  $W^\pm$  exchange produces  $\Sigma^\pm$  and  $\Sigma^0$  as shown in the middle diagram of Fig. 3. Meanwhile, at the electron-proton (ep)-collider,  $\Sigma^{0,\pm}$  are produced through vector-boson fusion process as shown in the right diagram of Fig. 3. Because all these processes only involves SM gauge interaction, their production cross section are solely determined by the heavy lepton triplet mass. Although there is no direct  $\Sigma^0$  pair production process, a pair of  $\Sigma^0$ s can be effectively generated from a pair production of  $\Sigma^\pm$  followed by  $\Sigma^\pm \rightarrow \Sigma^0 \pi^\pm$  decay, where the accompanying pion  $\pi^\pm$  is very soft and undetected.

For our analysis, we generate the signal sample with MADGRAPH5AMC@NLO [42,43] and evaluate the production cross section of the  $\Sigma^{0,\pm}$  at LHC, LHeC, and FCC-he. Our results are shown in Fig. 4 as a function of  $m_\Sigma$ . In the left panel of Fig. 4, we show the production cross section for the processes at the LHC with the center of mass energy  $\sqrt{s} = 13$  TeV. In the right panel of Fig. 4, we show the production cross section for the LHeC (FCC-he) collider, where the proton beam energy is set to be 7 (50) TeV while the  $e^-$  beam energy is set to be 60 GeV for both cases.

We now consider the decay of  $\Sigma^{\pm,0}$ . All the representative Feynman diagrams for the decay of  $\Sigma^0$  and  $\Sigma^\pm$  are shown in Fig. 5 and Fig. 6, respectively. The partial decay width of  $\Sigma^0$  to

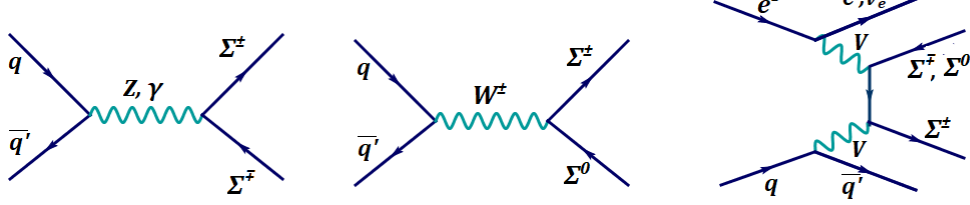


Figure 3: Representative Feynman diagrams for the production of  $\Sigma^\pm$  and  $\Sigma^0$  at colliders.

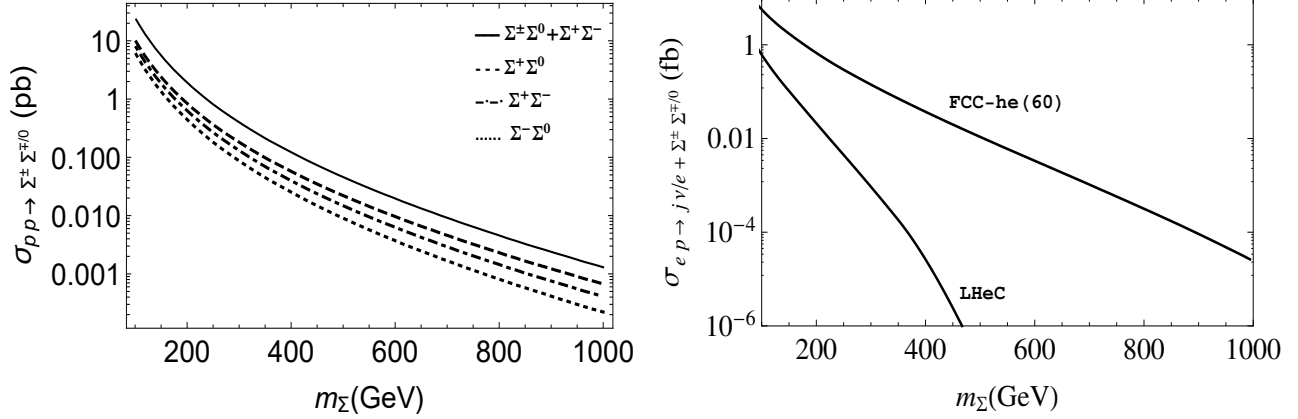


Figure 4: The left (right) shows the production cross section of  $\Sigma^\pm$  and  $\Sigma^0$  at pp(ep)-collider as a function of  $m_\Sigma$ .

SM Higgs ( $h$ ) and gauge bosons ( $Z, W^\pm$ ) are given by [44]

$$\begin{aligned}
 \Gamma(\Sigma_i^0 \rightarrow h\nu_\alpha) = \Gamma(\Sigma_i^0 \rightarrow h\bar{\nu}_\alpha) &= \frac{1}{8} \frac{M_\Sigma}{8\pi} \left( \frac{|R_{\alpha i}|^2}{2v^2} \right) \left( 1 - \frac{m_h^2}{M_\Sigma^2} \right)^2, \\
 \Gamma(\Sigma_i^0 \rightarrow Z\nu_\alpha) = \Gamma(\Sigma_i^0 \rightarrow Z\bar{\nu}_\alpha) &= \frac{1}{8} \frac{M_\Sigma}{8\pi} \left( \frac{|R_{\alpha i}|^2}{2v^2} \right) \left( 1 - \frac{2M_Z^2}{M_\Sigma^2} \right)^2 \left( 1 + \frac{2M_Z^2}{M_\Sigma^2} \right), \\
 \Gamma(\Sigma_i^0 \rightarrow W^+\ell_\alpha^-) = \Gamma(\Sigma_i^0 \rightarrow W^-\ell_\alpha^+) &= \frac{1}{4} \frac{M_\Sigma}{8\pi} \left( \frac{|R_{\alpha i}|^2}{2v^2} \right) \left( 1 - \frac{M_W^2}{M_\Sigma^2} \right)^2 \left( 1 + \frac{2M_W^2}{M_\Sigma^2} \right), \quad (3.1)
 \end{aligned}$$

where  $\alpha = e, \mu, \tau$  denotes different lepton flavors and

$$R_{\alpha i} = (m_D)_{\alpha i} (M_\Sigma)^{-1} = \frac{1}{\sqrt{m_\Sigma}} U_{\text{MNS}}^* \sqrt{D_\nu} O. \quad (3.2)$$

Similarly, the partial decay width of  $\Sigma^\pm$  to SM Higgs ( $h$ ) and gauge bosons ( $Z, W^\pm$ ) are

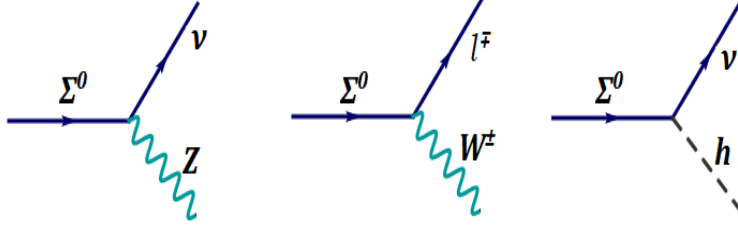


Figure 5: Representative Feynman diagrams for the decay of  $\Sigma^0$ .

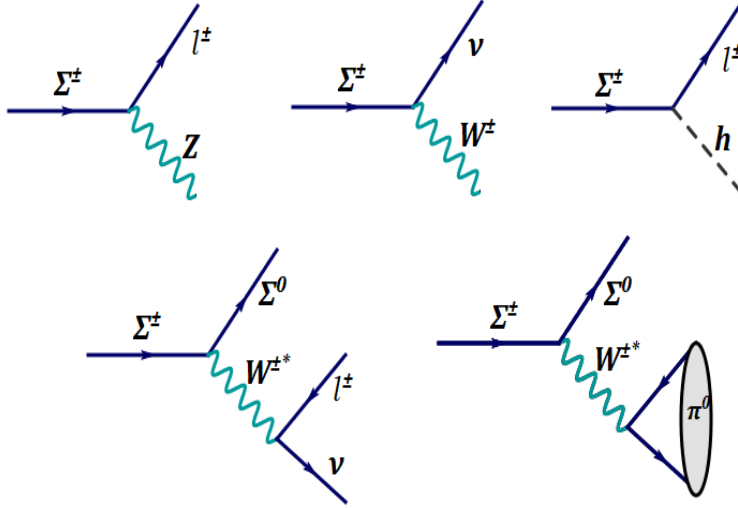


Figure 6: Representative Feynman diagrams for the decay of  $\Sigma^\pm$ .

given by [44]

$$\begin{aligned}
 \Gamma(\Sigma_i^\pm \rightarrow h \ell_\alpha^\pm) &= \frac{1}{4} \frac{M_\Sigma}{8\pi} \left( \frac{|R_{\alpha i}|^2}{2v^2} \right) \left( 1 - \frac{m_h^2}{M_\Sigma^2} \right)^2, \\
 \Gamma(\Sigma_i^\pm \rightarrow Z \ell_\alpha^\pm) &= \frac{1}{4} \frac{M_\Sigma}{8\pi} \left( \frac{|R_{\alpha i}|^2}{2v^2} \right) \left( 1 - \frac{M_Z^2}{M_\Sigma^2} \right)^2 \left( 1 + \frac{2M_Z^2}{M_\Sigma^2} \right), \\
 \Gamma(\Sigma_i^\pm \rightarrow W^\pm \bar{\nu}_\alpha) &= \frac{1}{2} \frac{M_\Sigma}{8\pi} \left( \frac{|R_{\alpha i}|^2}{2v^2} \right) \left( 1 - \frac{2M_W^2}{M_\Sigma^2} \right)^2 \left( 1 + \frac{2M_W^2}{M_\Sigma^2} \right). \tag{3.3}
 \end{aligned}$$

Because of the mass-splitting  $\Sigma^\pm$  can also decay into  $\Sigma^0$  and pions or light leptons; the corre-

sponding partial decay widths for the processes are given by [44]

$$\begin{aligned}
\Gamma(\Sigma_i^\pm \rightarrow \Sigma_i^0 \pi^\pm) &= \frac{2G_F^2 V_{ud}^2 \Delta M^3 f_\pi^2}{\pi} \sqrt{1 - \frac{m_\pi^2}{\Delta M^2}}, \\
\Gamma(\Sigma_i^\pm \rightarrow \Sigma_i^0 e^\pm \bar{\nu}_e) &= \frac{2G_F^2 \Delta M^5}{15\pi^3}, \\
\Gamma(\Sigma_i^\pm \rightarrow \Sigma_i^0 \mu^\pm \bar{\nu}_\mu) &= 0.12 \Gamma(\Sigma_i^\pm \rightarrow \Sigma_i^0 e^\pm \bar{\nu}_e).
\end{aligned} \tag{3.4}$$

From Eqs. (3.1), (3.2), (3.3) and (3.4), together with the fact that observed light neutrino mass spectrum is uniquely determined by the lightest neutrino mass  $m_{lightest} = m_1(m_3)$ , for NH (IH), it is clear that all the partial decay widths are determined by only two free parameters ( $m_\Sigma, m_{lightest}$ ), and the complex angles  $\theta_{1,2,3}$ . For the special case,  $\theta_{1,2,3} = 0$ , or equivalently  $O$  is a unit  $3 \times 3$  matrix,  $|R_{\alpha i}|^2 = m_i/m_\Sigma$  [34].

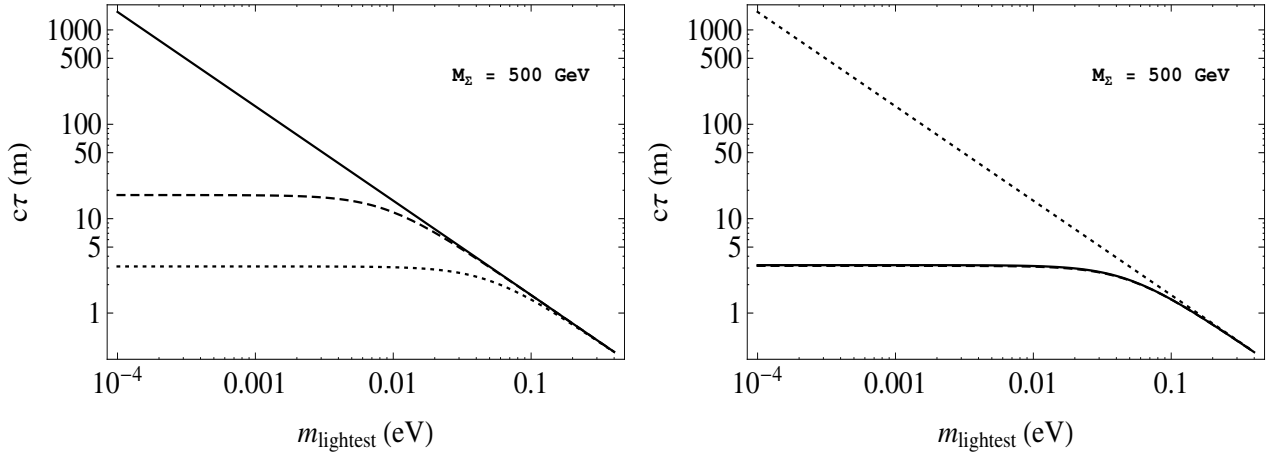


Figure 7: For  $\theta_{1,2,3} = 0$  and  $m_\Sigma = 500$  GeV, the plots show the decay length of the neutral fermion ( $\Sigma_i^0$ ) as a function of lightest observed neutrino mass. The left (right) panel corresponds to the NH (IH) case: solid, dashed, and dotted lines correspond to the decay length of  $\Sigma_1^0$  ( $\Sigma_3^0$ ),  $\Sigma_2^0$  ( $\Sigma_1^0$ ), and  $\Sigma_3^0$  ( $\Sigma_2^0$ ), respectively, with  $m_{lightest} = m_1$  ( $m_3$ ).

Let us now estimate the decay length of  $\Sigma^{0,\pm}$ , which is given by  $c\tau = 1/\Gamma_{total}^{\pm,0}$ , where  $\Gamma_{total}^{\pm,0}$  is the total decay width of  $\Sigma^{0,\pm}$ , respectively. We consider two cases,  $\theta_{1,2,3} = 0$  and  $\theta_{1,2,3} \neq 0$ , separately. In Fig. 7, we consider the case  $O = \mathbf{1}$  ( $\theta_{1,2,3} = 0$ ) and plot the decay length of  $\Sigma^0$  as a function of lightest neutrino mass ( $m_{lightest}$ ). The left (right) panel corresponds to the NH (IH) case. Here, the solid, dashed, and dotted lines correspond to the decay length of  $\Sigma_1^0$  ( $\Sigma_3^0$ ),  $\Sigma_2^0$  ( $\Sigma_1^0$ ), and  $\Sigma_3^0$  ( $\Sigma_2^0$ ), respectively, with  $m_{lightest} = m_1$  ( $m_3$ ). As mentioned earlier, when the orthogonal matrix  $O$  is a unit  $3 \times 3$  matrix ( $\theta_{1,2,3} = 0$ ),  $|R_{\alpha i}|^2 = m_i/m_\Sigma$  and hence the partial decay widths of  $\Sigma_i^0$  in Eq. (3.1) are independent of  $m_\Sigma$ . We see in Fig. 7 that the decay length of  $\Sigma_1^0$  ( $\Sigma_3^0$ ) for NH (IH) is inversely proportional to  $m_{lightest} = m_1$  ( $m_3$ ). In the limit  $m_{lightest} \rightarrow 0$ , the other light neutrino masses approach constant values, so that the other  $\Sigma^0$ 's decay lengths become constant.



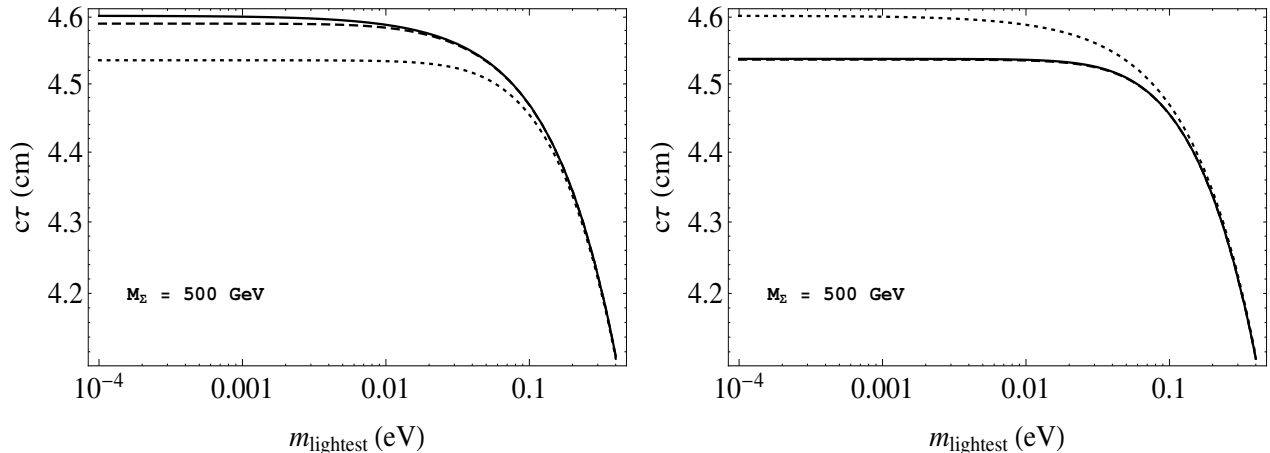


Figure 8: For  $\theta_{1,2,3} = 0$  and  $m_\Sigma = 500$  GeV, the plots show the decay length of the neutral fermion ( $\Sigma_i^\pm$ ) as a function of lightest observed neutrino mass: The left (right) panel corresponds to the NH (IH) case: solid, dashed, and dotted lines correspond to the decay length of  $\Sigma_1^\pm$  ( $\Sigma_3^\pm$ ),  $\Sigma_2^\pm$  ( $\Sigma_2^\pm$ ), and  $\Sigma_3^\pm$  ( $\Sigma_1^\pm$ ), respectively, with  $m_{lightest} = m_1$  ( $m_3$ ).

In Fig. 8, for  $\theta_{1,2,3} = 0$ , we show the decay length of the charged fermions ( $\Sigma_i^\pm$ ) as a function of  $m_{lightest}$ . The line codings are the same as Fig. 7. In the limit  $m_{lightest} \rightarrow 0$ , the charged fermion ( $\Sigma^\pm$ ) dominantly decays into  $\Sigma^0$ , hence its decay width is determined by  $\Delta M$ . As shown in Fig. 1,  $\Delta M \simeq 170$  MeV for  $m_\Sigma = 500$  GeV, and the decay lengths approach constant values in the limit  $m_{lightest} \rightarrow 0$ . This fact explains the observation that the decay length of charged fermions is much smaller than the neutral fermion one.

Next, we consider the case  $\theta_{1,2,3} \neq 0$ . Let us parameterize  $\theta_1 = x_1 + iy_1$ ,  $\theta_2 = x_2 + iy_2$ , and  $\theta_3 = x_3 + iy_3$ . In the following we set  $x_{1,2,3} = 0$  for simplicity. In this case,  $\cos(x_i + iy_i) \simeq \sin(x_i + iy_i) \simeq e^{y_i}$  for  $y_i \gtrsim 1$ . Hence,  $|R_{\alpha i}|^2$  can be exponentially enhanced for nonzero values of  $y$ . To see this effect, we consider the charged fermion  $\Sigma^\pm$  decay in the following. Because of the exponential enhancement, the total decay width of  $\Sigma^\pm$  is dominated by its decay to  $W^\pm$ ,  $Z$  and  $h$ . The result is shown in Fig. 9 for  $y_{1,2,3} = 2.5$  and  $m_\Sigma = 500$  GeV. The line codings are the same as Fig. 8. The plot shows huge suppression of the decay length compared to the unit orthogonal matrix case considered in Fig. 8. The exponential constant suppression explains an almost constant decay length in the limit  $m_{lightest} \rightarrow 0$ . Also, because  $|R_{\alpha i}|^2 \times m_\Sigma$  is effectively independent of  $m_\Sigma$ , the dependence of the decay length on  $m_\Sigma$  is very weak.

We briefly comment on the decay length of  $\Sigma^0$  for  $\theta_{1,2,3} \neq 0$ . For definiteness, let us consider  $x_{1,2,3} = 0$ ,  $y_{1,2,3} = 2.5$ , and  $m_\Sigma = 500$  GeV. For these values, as we have discussed earlier, the total decay width of  $\Sigma^\pm$  is dominated by its decay to  $W^\pm$ ,  $Z$  and  $h$ . Since the total decay width of  $\Sigma^0$  and  $\Sigma^\pm$  to  $W^\pm$ ,  $Z$  and  $h$  are identical with  $\Delta M \ll m_\Sigma$ , the decay length of  $\Sigma^0$  is the same as that in Fig. 8.

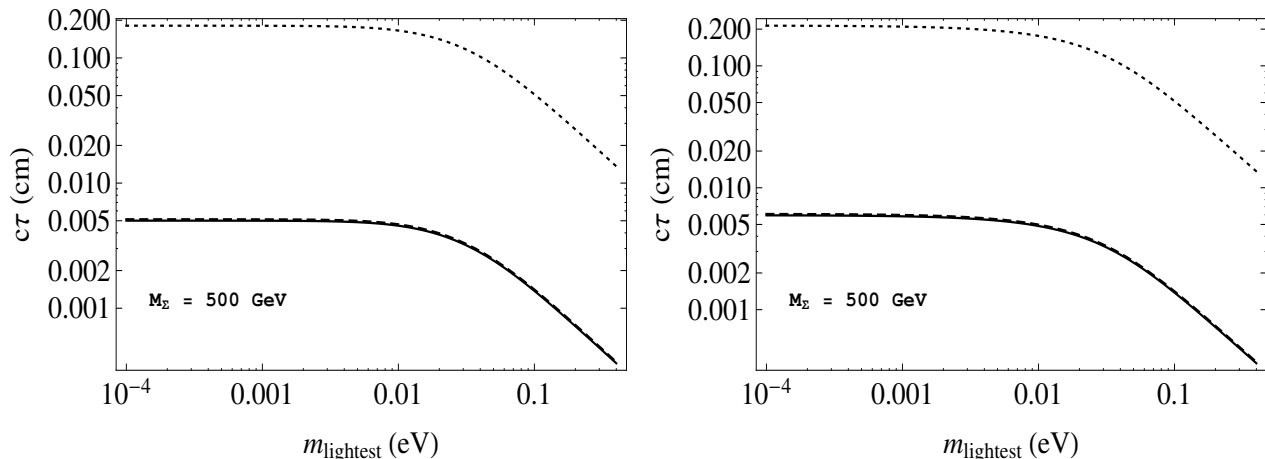


Figure 9: For  $\theta_{1,2,3} \neq 0$  (see text for details) and  $m_\Sigma = 500$  GeV, the plots show the decay length of the neutral fermion ( $\Sigma_i^\pm$ ) as a function of lightest observed neutrino mass: The left (right) panel corresponds to the NH (IH) case: solid, dashed, and dotted lines correspond to the decay length of  $\Sigma_1^\pm$  ( $\Sigma_3^\pm$ ),  $\Sigma_2^\pm$  ( $\Sigma_1^\pm$ ), and  $\Sigma_3^\pm$  ( $\Sigma_2^\pm$ ), respectively, with  $m_{\text{lightest}} = m_1$  ( $m_3$ ).

## 4 Displaced vertex signals at current/future colliders

In the following, we will examine the prospect of probing the type-III seesaw scenario at various current and planned collider experiments using disappearing track searches and displaced vertex searches.

### 4.1 Disappearing track searches for $\Sigma^\pm$ at the LHC

As discussed before, radiative corrections generate mass-splitting between the charged ( $\Sigma^\pm$ ) and neutral ( $\Sigma^0$ ) fermions with a mass difference of the order of pion mass. Hence, the heavier  $\Sigma^\pm$  can decay into  $\Sigma^0$  emitting a soft pion. Since  $\Sigma^0$  is a SM singlet and the soft pion is hard to reconstruct,  $\Sigma^\pm$  track disappears if it decays inside the detector. This is so-called disappearing track signal and the LHC experiments have yet to observe such a signal from particles beyond the SM [13].

In the left panel of Fig. 10, we show the production cross section for  $\Sigma^{\pm,0}$  as a function of  $M_\Sigma$  (red line) obtained in Fig. 4, together with the upper bound on the production cross section of the charged fermions obtained from disappearing track search by CMS [11]. The production cross section of  $\Sigma^0\Sigma^\pm$  ( $\Sigma^\mp\Sigma^\pm$ ) at the LHC is depicted by solid (dashed) blue curves. For different  $c\tau$  values, the green (yellow) band in each of the plot are the current upper bound on the production cross section at 2(3)- $\sigma$  confidence level.

In the right panel of Fig. 10, we recast the prospect of a long-lived charged Higgsino search at the HL-LHC using its disappearing track signature. If we identify the charged (neutral) component of Higgsino with  $\Sigma^\pm$  ( $\Sigma^0$ ), the production mechanism for charged Higgsino in Ref. [45] is exactly the same as  $\Sigma^\pm$  in our case in Fig. 3. In our analysis we have taken this into account

that the production cross section of Higgsino is slightly different to our case. The red horizontal lines depicts the lifetime of a  $\Sigma_i^\pm$ s as a function of  $m_\Sigma$ . Here, we have considered NH case with a unit orthogonal matrix, and  $m_{lightest} = 10^{-3}$  eV. In the plot the lifetime of all  $\Sigma_{1,2,3}^\pm$  very much overlap with each other. For the IH case, the ordering of lifetime for  $\Sigma_i^\pm$  changes but its values is almost the same as the NH case, see, Fig. 8.

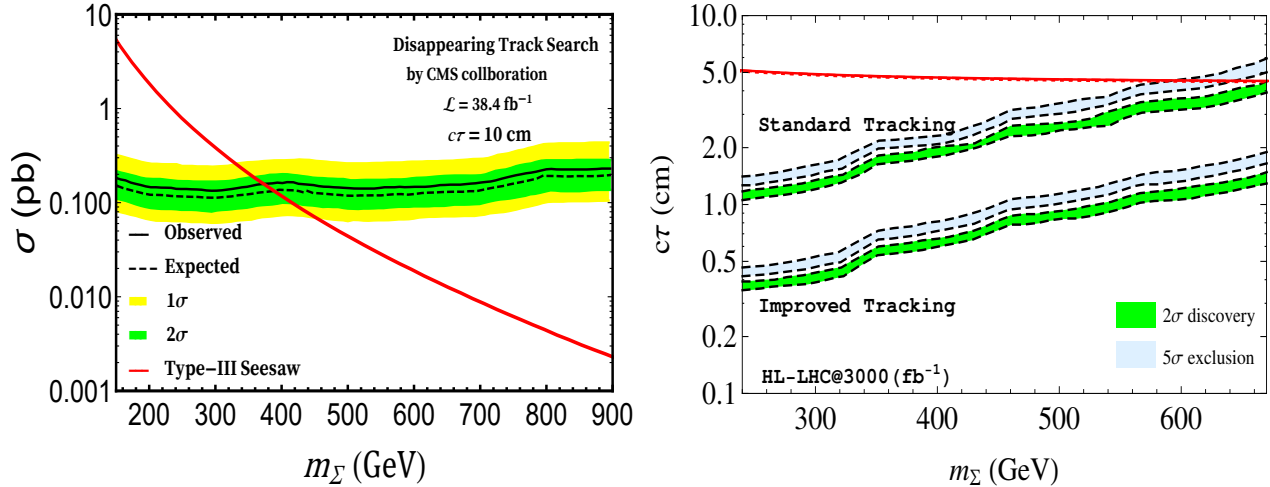


Figure 10: The left panel shows the current limit on mass of  $\Sigma^\pm$  from the search for the signature of a disappearing track by CMS collaboration. The expected and observed 95% CL upper bounds on the product of the cross section of direct  $\Sigma^\pm$  production and branching fraction to  $\Sigma^0\pi^\pm$  as a function of fermion triplet mass for fixed lifetime  $c\tau = 10$  cm. The direct  $\Sigma^\pm$  production cross section includes both  $\Sigma^0\Sigma^\pm$  and  $\Sigma^\pm\Sigma^\mp$  production. In the right panel, we show the disappearing track search reach at the HL-LHC with  $3000 \text{ fb}^{-1}$  luminosity.

## 4.2 $\Sigma^0$ search at MATHUSLA

The recently, proposed MATHUSLA [31] is purposefully designed to detect long-lived particles produced at the LHC, and will be located  $\sim 100$  m at an angle  $\theta = [0.38, 0.8]$  away from the LHC beam. Hence, it is ideally suited to detect long-lived particles with their decay lengths in the range of few hundred meters or even longer [46]. If the particle decays with final state charged leptons and/or jets, the event can be easily reconstructed because the background SM events will be almost zero.

We have earlier shown in Fig. 7 that the charge neutral  $\Sigma^0$  particle can have decay length of  $\mathcal{O}(100)$  m. In the following, we investigate a possibility of detecting  $\Sigma^0$  at MATHUSLA. At LHC,  $\Sigma^0$  is produced in two ways. One is from  $\Sigma^\pm$  production through a  $s$ -channel  $Z/\gamma$  in the left diagram of Fig. 3, and the other is through  $s$ -channel  $W^\pm$  exchange process in the middle diagram of Fig. 3. In the first case, one  $\Sigma^0$  is directly produced while in the other  $\Sigma^0$  is produced by  $\Sigma^\pm$  decay. The other particles produced from  $\Sigma^\pm$  decay are too soft and will not be considered in our analysis. Note that these processes are different from the resonant production of long-lived particles generally considered in the MATHUSLA studies. Since the

MATHUSLA detector is very efficient in detecting long-lived particles, we will simply require that one  $\Sigma^0$  particle produced at the LHC reaches the MATHUSLA detector and decays. In the following, we assume that the decaying  $\Sigma^0$  particle can be detected with 100% efficiency by MATHUSLA because the SM backgrounds are negligible.

Let us assume that  $\Sigma^0$  produced at the LHC is emitted at an angle of  $\theta$  away from the LHC beam such that it decays after traveling a distance of  $D_M$ . Hence, its decay length in the laboratory frame is given by

$$c\tau_{\text{lab}} = \frac{D_M}{\beta}. \quad (4.1)$$

Here, the  $\beta$  is the boost factor for  $\Sigma^0$  particle,

$$\beta = \frac{1}{\sqrt{1 + \frac{m_\Sigma^2}{\vec{P}_{\text{tot}}^2}}}, \quad (4.2)$$

with a total momentum  $\vec{P}_{\text{tot}} = p_T \cosh \eta$ , where  $p_T$  is  $\Sigma^0$ 's transverse momentum and  $\eta = -\ln[\tan(\theta/2)]$  is its rapidity. Hence, the proper decay length  $c\tau$  of the particle is given by

$$c\tau = c\tau_{\text{lab}} \times \sqrt{1 - \beta^2} = D_M \frac{\sqrt{1 - \beta^2}}{\beta}. \quad (4.3)$$

Let us fix  $D_M = 100$  m and set  $\theta \simeq 0.5$  corresponding to the location of the MATHUSLA detector. Hence,  $P_{\text{tot}} \simeq 2p_T$  and

$$c\tau \simeq 2D_M \left( \frac{m_\Sigma}{p_T} \right) = 200 \left( \frac{m_\Sigma}{p_T} \right). \quad (4.4)$$

To simulate the production of  $\Sigma^0$  observed by MATHUSLA, we employ MADGRAPH5AMC @NLO [42, 43] and calculated the production cross section ( $\sigma$ ) for the process. In the top left (right) panel of Fig. 11, for  $m_\Sigma = 200$  (500) GeV, we show the cross section as a function of transverse momentum ( $p_T$ ) of  $\Sigma_0$ . Because of low background, let us require 25 events ( $N = 25$ ) for a “ $\Sigma^0$  discovery” by MATHUSLA. In the bottom left (right) panel of Fig. 11, for  $m_\Sigma = 200$  (500) GeV, we show the luminosity ( $\mathcal{L} = N/\sigma$ ) required for such a discovery of  $\Sigma_0$  as a function of its decay length, which we evaluated using Eq. (4.4). The top (bottom) horizontal line denotes the integrated luminosity at HL-LHC with  $\mathcal{L} = 300$  (3000)  $\text{fb}^{-1}$ . From the bottom panels we find that the MATHUSLA can discover  $\Sigma^0$  with a mass 200 GeV and 500 GeV, if their decay lengths are in the range  $\mathcal{O}(10^2)m - \mathcal{O}(10^4)m$  and  $\mathcal{O}(10^2)m - \mathcal{O}(10^3)m$ , respectively. Because the cross section decreases with increasing  $m_\Sigma$  values, a heavier  $\Sigma_0$  requires higher luminosity, for example, we find that  $m_\Sigma = 1000$  GeV requires  $\mathcal{L} > 3000 \text{ fb}^{-1}$  for any  $c\tau$  values.

### 4.3 $\Sigma^\pm$ search at LHeC and FCC-he

Let us now consider the displaced vertex signature arising from the charged fermion  $\Sigma^\pm$  decay at ep-colliders. Authors in Ref. [47] have studied such the prospect to detect charged Higgsinos at LHeC and FCC-he experiments. If we identify the charged (neutral) component of Higgsino

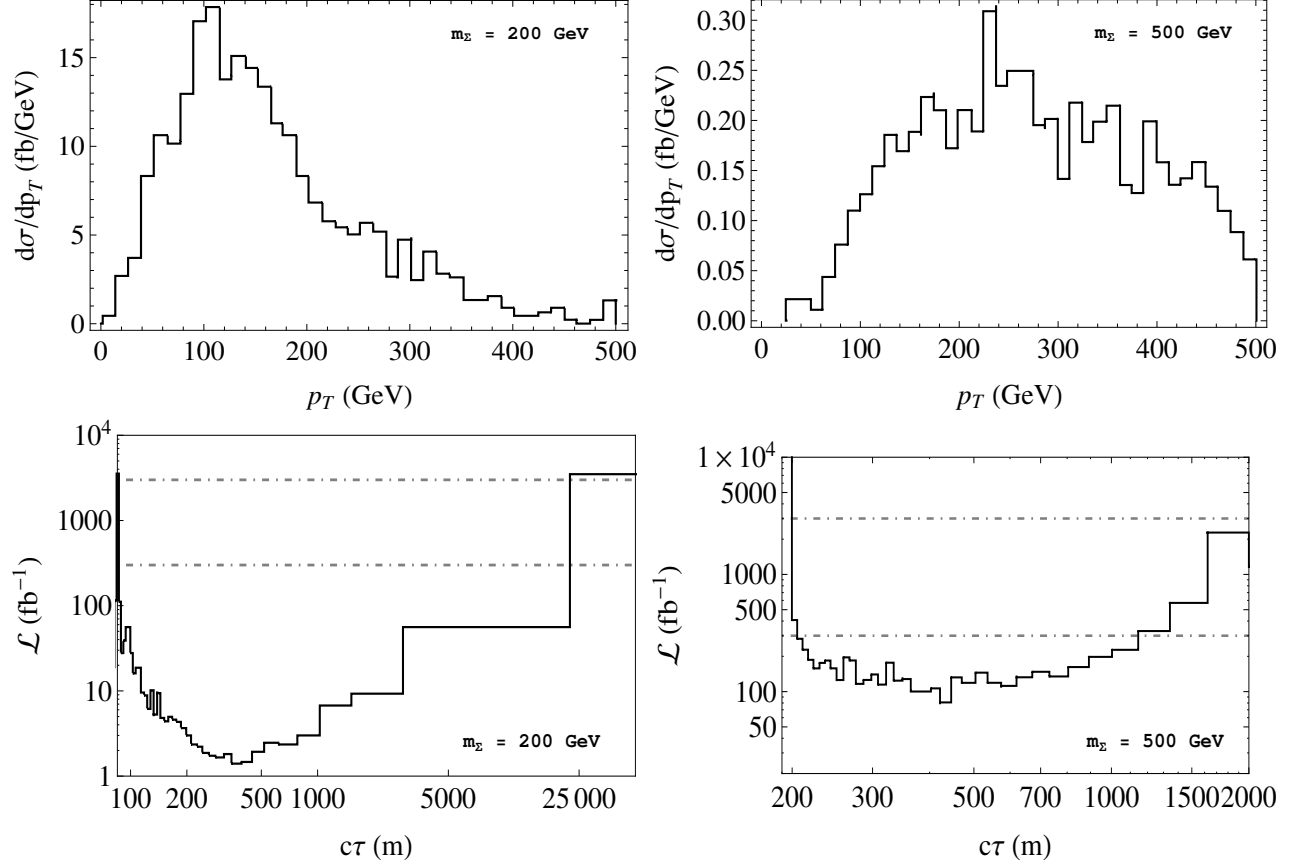


Figure 11: The top left (right) show the production cross section as a function of  $p_T$  for  $m_\Sigma = 200$  (500) GeV. In the bottom panels, we show the luminosities required to produce 25  $\Sigma^0$  at LHC which are directed towards MATHUSLA, and the horizontal top (bottom) line denote  $\mathcal{L} = 300$  (3000)  $\text{fb}^{-1}$ .

with  $\Sigma^\pm$  ( $\Sigma^0$ ), the production mechanism for charged Higgsino is exactly the same as  $\Sigma^\pm$  in our case in Fig. 3. However, there are two important differences between the two scenarios: the obvious one is the difference in the production cross sections of Higgsino and  $\Sigma$ , the other is the decay length. For the charged Higgsino, the mass-splitting between the charged and neutral Higgsinos, which determines the decay lengths is essentially a free parameter. For example, a decay length in the range of  $10^{-3}$ -10 cm, which is suitable for FCC-he and LHeC search, requires Higgsino mass-splitting in the range of 0.2-2 GeV [47]. As discussed in Sec. 3, if the orthogonal matrix is a unit matrix,  $\Sigma^\pm$  decay length is primarily determined by the mass-splitting between  $\Sigma^\pm$  and  $\Sigma^0$ . However, the mass-splitting is very small,  $\Delta M \simeq 0.1$  GeV, for example  $c\tau \simeq 4$  cm for  $m_\Sigma = 500$  GeV, see, Fig. 8. Meanwhile, if the orthogonal matrix  $O$  is allowed to be complex,  $\Sigma^\pm$  can have a decay length as small as  $10^{-3}$  cm (see, Fig. 9).

In Fig. 10, we recast the prospect of a long-lived charged Higgsino search at the LHeC (top panel) and FCC-he (bottom panels) to our case. The corresponding luminosities are indicated in each plots. In each plots, the blue and green shaded regions indicate the parameter space

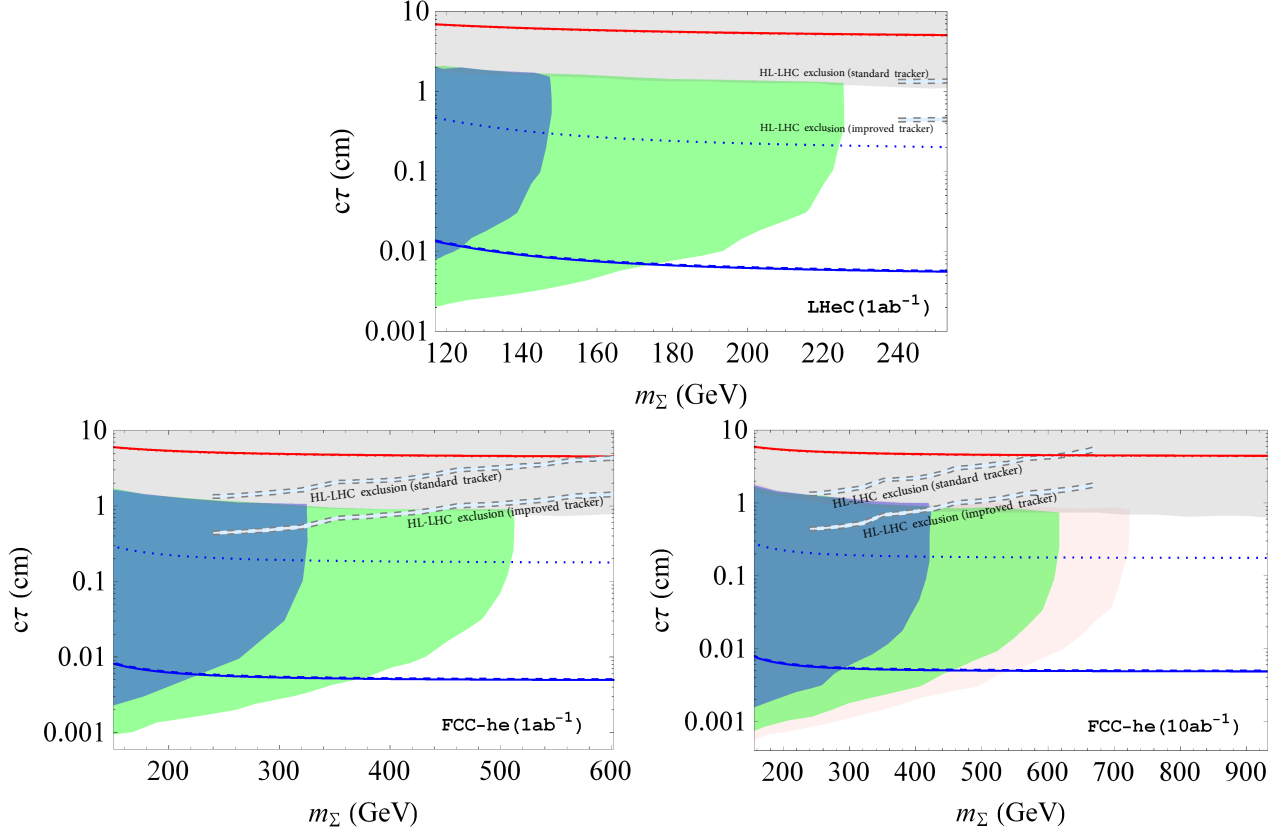


Figure 12: The prospect of observing displaced vertex from  $\Sigma^\pm$  decay at LHeC (top panel) and FCC-he (bottom panels). The blue and green shaded regions indicate the parameter space where 10 (100) events with least one long-lived  $\Sigma^\pm$  observed at the LHeC/FCC-he. The light-red shaded regions indicate 2- $\sigma$  exclusion sensitivity if the backgrounds are harder to reject. The grey shaded region are still allowed. For the NH case with a unit (complex) orthogonal matrix, the red (blue) horizontal lines indicate the decay length for  $m_{lightest} = 10^{-3}$  eV. The dashed diagonal lines are 5- $\sigma$  exclusion reach of HL-LHC from the disappearing track searches.

where 10 (100) events with least one long-lived  $\Sigma^\pm$  is observed at the LHeC/FCC-he; the green shaded regions correspond to 2- $\sigma$  exclusion sensitivity. In the bottom right plot, the red shaded regions 2- $\sigma$  exclusion sensitivity if the backgrounds are harder to reject. The grey shaded region in all the plots have no significance to our case and the parameter region is still allowed. In our analysis, we have taken into account the difference between the production cross section of Higgsino and  $\Sigma$ .

In each plot of Fig. 12, we also show the lifetime of  $\Sigma_i^\pm$  as a function of  $m_\Sigma$  for a fixed lightest neutrino mass,  $m_{lightest} = 10^{-3}$  eV. Here, for example, the red horizontal lines indicate the result for the NH case with a unit orthogonal matrix. In the figure, lifetimes of all  $\Sigma_{1,2,3}^\pm$  very much overlap with each other. Meanwhile, the blue solid, dashed, and dotted line indicate the decay length of  $\Sigma_{1,2,3}^\pm$ , respectively, using a complex orthogonal matrix with  $x_{1,2,3} = 0$  and  $y_{1,2,3} = 2.5$ . Also, we show the 5- $\sigma$  exclusion reach of HL-LHC obtained in the right panel of

Fig. 10 from the disappearing track searches.

## 5 Summary

We have investigated the prospect of probing the type III seesaw neutrino mass generation mechanism at various collider experiments by searching for a disappearing track signature as well as a displaced vertex signature originating from the decay of  $SU(2)_L$  triplet fermion  $\Sigma$ . Because  $\Sigma$  is primarily produced at colliders through their electroweak gauge interactions, its production rate is uniquely determined by its mass  $m_\Sigma$ . The triplet fermion include one neutral component,  $\Sigma^0$ , and two charged components,  $\Sigma^\pm$ . The type-III seesaw mechanism generates the observed neutrinos masses, which together with  $m_\Sigma$ , determine the decay length of  $\Sigma^{0,\pm}$ . The charged fermion  $\Sigma^\pm$  with decay length of  $c\tau = \mathcal{O}(5)$  cm can decay emitting a soft pion and can be observed with a disappearing track search at the LHC and HL-LHC. Furthermore, their displaced vertex signature can also be observed by proposed colliders such as FCC-he and LHeC. For a certain choice of parameters,  $\Sigma^\pm$  can have a much shorter lifetime,  $c\tau \simeq 10^{-3}$  cm. Although such a small decay width is beyond the reach of disappearing track searches, they can still produce a displaced vertex signal which can be observed by FCC-he and LHeC. On the other hand, the decay length of  $\Sigma^0$  associated with the lightest neutrino is inversely proportional to the lightest neutrino mass  $m_{lightest}$ . As a result, with  $10^{-4} \lesssim m_{lightest}/\text{eV} \lesssim 10^{-3}$  its decay length can be much longer,  $10^2 \lesssim c\tau/m \lesssim 10^3$ . This is ideal for the MATHUSLA detector. We have shown that  $\Sigma^0$  particle with a mass of a few hundred GeV can easily produce sufficient number of decay events to be discovered by MATHUSLA.

## 6 Acknowledgement

We thank Oliver Fischer for helpful discussions. This work is supported in part by the United States Department of Energy grant de-sc0012447 (N.O) and de-sc0013880 (D.R).

## References

- [1] Q. R. Ahmad *et al.* [SNO Collaboration], Phys. Rev. Lett. **89**, 011301 (2002) [nucl-ex/0204008]; Q. R. Ahmad *et al.* [SNO Collaboration], Phys. Rev. Lett. **89**, 011302 (2002) [nucl-ex/0204009]; J. Hosaka *et al.* [Super-Kamiokande Collaboration], Phys. Rev. D **74**, 032002 (2006) [hep-ex/0604011]; K. Eguchi *et al.* [KamLAND Collaboration], Phys. Rev. Lett. **90**, 021802 (2003) [hep-ex/0212021]; M. H. Ahn *et al.* [K2K Collaboration], Phys. Rev. Lett. **90**, 041801 (2003) [hep-ex/0212007]; K. Abe *et al.* [T2K Collaboration], Phys. Rev. Lett. **107**, 041801 (2011) [arXiv:1106.2822 [hep-ex]].
- [2] P. Minkowski, Phys. Lett. B **67** (1977) 421; T. Yanagida, *Proceedings of the Workshop on the Unified Theory and the Baryon Number in the Universe*, eds. O. Sawada et al., p. 95, KEK Report 79-18, Tsukuba (1979); M. Gell-Mann, P. Ramond and R. Slansky, in *Supergravity*, eds. P. van Nieuwenhuizen et al., (North-Holland, 1979), p. 315; S.L. Glashow, in *Quarks and Leptons*, Cargèse, eds. M. Lévy et al., (Plenum, 1980), p. 707.

- [3] R. N. Mohapatra and G. Senjanović, Phys. Rev. Lett. **44** (1980) 912.
- [4] W. Konetschny and W. Kummer, Phys. Lett. B **70** (1977) 433; T. P. Cheng and L. F. Li, Phys. Rev. D **22** (1980) 2860; G. Lazarides, Q. Shafi and C. Wetterich, Nucl. Phys. B **181** (1981) 287; J. Schechter and J. W. F. Valle, Phys. Rev. D **22** (1980) 2227; R. N. Mohapatra and G. Senjanović, Phys. Rev. D **23** (1981) 165.
- [5] R. Foot, H. Lew, X. G. He and G. C. Joshi, Z. Phys. C **44** (1989) 441.
- [6] E. Ma, Phys. Rev. Lett. **81** (1998) 1171. [arXiv:hep-ph/9805219].
- [7] B. Bajc and G. Senjanović, JHEP **0708** (2007) 014. [arXiv:hep-ph/0612029].
- [8] P. Fileviez Pérez, Phys. Lett. B **654** (2007) 189; Phys. Rev. D **76** (2007) 071701. [arXiv:0705.3589 [hep-ph]].
- [9] A. Arhrib, B. Bajc, D. K. Ghosh, T. Han, G. Y. Huang, I. Puljak and G. Senjanovic, Phys. Rev. D **82**, 053004 (2010) [arXiv:0904.2390 [hep-ph]].
- [10] R. Franceschini, T. Hambye and A. Strumia, Phys. Rev. D **78**, 033002 (2008) [arXiv:0805.1613 [hep-ph]].
- [11] A. M. Sirunyan *et al.* [CMS Collaboration], Phys. Rev. Lett. **119**, no. 22, 221802 (2017) [arXiv:1708.07962 [hep-ex]].
- [12] The ATLAS collaboration [ATLAS Collaboration], ATLAS-CONF-2018-020.
- [13] M. Aaboud *et al.* [ATLAS Collaboration], “Search for long-lived charginos based on a disappearing-track signature in pp collisions at  $\sqrt{s} = 13$  TeV with the ATLAS detector,” JHEP **1806**, 022 (2018) [arXiv:1712.02118 [hep-ex]].
- [14] G. Aad *et al.* [ATLAS Collaboration], Phys. Rev. Lett. **108**, 251801 (2012)
- [15] S. Chatrchyan *et al.* [CMS Collaboration], “Search for heavy long-lived charged particles in  $pp$  collisions at  $\sqrt{s} = 7$  TeV,”
- [16] G. Aad *et al.* [ATLAS Collaboration], “Search for displaced muonic lepton jets from light Higgs boson decay in proton-proton collisions at  $\sqrt{s} = 7$  TeV with the ATLAS detector,” Phys. Lett. B **721**, 32 (2013) [arXiv:1210.0435 [hep-ex]].
- [17] G. Aad *et al.* [ATLAS Collaboration], “Search for long-lived, heavy particles in final states with a muon and multi-track displaced vertex in proton-proton collisions at  $\sqrt{s} = 7$  TeV with the ATLAS detector,” Phys. Lett. B **719**, 280 (2013) [arXiv:1210.7451 [hep-ex]].
- [18] S. Chatrchyan *et al.* [CMS Collaboration], “Search in leptonic channels for heavy resonances decaying to long-lived neutral particles,” JHEP **1302**, 085 (2013) [arXiv:1211.2472 [hep-ex]].



- [19] G. Aad *et al.* [ATLAS Collaboration], “Search for long-lived neutral particles decaying into lepton jets in proton-proton collisions at  $\sqrt{s} = 8$  TeV with the ATLAS detector,” JHEP **1411**, 088 (2014) [arXiv:1409.0746 [hep-ex]].
- [20] V. Khachatryan *et al.* [CMS Collaboration], “Search for Long-Lived Neutral Particles Decaying to Quark-Antiquark Pairs in Proton-Proton Collisions at  $\sqrt{s} = 8$  TeV,” Phys. Rev. D **91**, no. 1, 012007 (2015) [arXiv:1411.6530 [hep-ex]].
- [21] V. Khachatryan *et al.* [CMS Collaboration], “Search for long-lived particles that decay into final states containing two electrons or two muons in proton-proton collisions at  $\sqrt{s} = 8$  TeV,” Phys. Rev. D **91**, no. 5, 052012 (2015) [arXiv:1411.6977 [hep-ex]].
- [22] R. Aaij *et al.* [LHCb Collaboration], “Search for long-lived particles decaying to jet pairs,” Eur. Phys. J. C **75**, no. 4, 152 (2015) [arXiv:1412.3021 [hep-ex]].
- [23] G. Aad *et al.* [ATLAS Collaboration], “Search for pair-produced long-lived neutral particles decaying in the ATLAS hadronic calorimeter in  $pp$  collisions at  $\sqrt{s} = 8$  TeV,” Phys. Lett. B **743**, 15 (2015) [arXiv:1501.04020 [hep-ex]].
- [24] G. Aad *et al.* [ATLAS Collaboration], “Search for long-lived, weakly interacting particles that decay to displaced hadronic jets in proton-proton collisions at  $\sqrt{s} = 8$  TeV with the ATLAS detector,” Phys. Rev. D **92**, no. 1, 012010 (2015) [arXiv:1504.03634 [hep-ex]].
- [25] G. Aad *et al.* [ATLAS Collaboration], “Search for massive, long-lived particles using multitrack displaced vertices or displaced lepton pairs in  $pp$  collisions at  $\sqrt{s} = 8$  TeV with the ATLAS detector,” Phys. Rev. D **92**, no. 7, 072004 (2015) [arXiv:1504.05162 [hep-ex]].
- [26] M. Aaboud *et al.* [ATLAS Collaboration], “Search for metastable heavy charged particles with large ionization energy loss in  $pp$  collisions at  $\sqrt{s} = 13$  TeV using the ATLAS experiment,” Phys. Rev. D **93**, no. 11, 112015 (2016) [arXiv:1604.04520 [hep-ex]].
- [27] M. Aaboud *et al.* [ATLAS Collaboration], “Search for heavy long-lived charged  $R$ -hadrons with the ATLAS detector in  $3.2 \text{ fb}^{-1}$  of proton–proton collision data at  $\sqrt{s} = 13$  TeV,” Phys. Lett. B **760**, 647 (2016) [arXiv:1606.05129 [hep-ex]].
- [28] The ATLAS collaboration [ATLAS Collaboration], “Search for long-lived neutral particles decaying into displaced lepton jets in proton–proton collisions at  $\sqrt{s} = 13$  TeV with the ATLAS detector,” ATLAS-CONF-2016-042.
- [29] The ATLAS collaboration [ATLAS Collaboration], “Search for long-lived neutral particles decaying in the hadronic calorimeter of ATLAS at  $\sqrt{s} = 13$  TeV in  $3.2 \text{ fb}^{-1}$  of data,” ATLAS-CONF-2016-103.
- [30] M. Aaboud *et al.* [ATLAS Collaboration], “Search for long-lived, massive particles in events with displaced vertices and missing transverse momentum in  $\sqrt{s} = 13$  TeV  $pp$  collisions with the ATLAS detector,” Phys. Rev. D **97**, no. 5, 052012 (2018) [arXiv:1710.04901 [hep-ex]].

- [31] J. P. Chou, D. Curtin and H. J. Lubatti, “New Detectors to Explore the Lifetime Frontier,” *Phys. Lett. B* **767**, 29 (2017) [arXiv:1606.06298 [hep-ph]].
- [32] J. L. Abelleira Fernandez *et al.* [LHeC Study Group], “A Large Hadron Electron Collider at CERN: Report on the Physics and Design Concepts for Machine and Detector,” *J. Phys. G* **39**, 075001 (2012) [arXiv:1206.2913 [physics.acc-ph]].
- [33] M. Kuze, “Energy-Frontier Lepton-Hadron Collisions at CERN: the LHeC and the FCC-he,”
- [34] S. Jana, N. Okada and D. Raut, “Displaced vertex signature of type-I seesaw model,” *Phys. Rev. D* **98**, no. 3, 035023 (2018) [arXiv:1804.06828 [hep-ph]].
- [35] J. C. Helo, M. Hirsch and S. Kovalenko, “Heavy neutrino searches at the LHC with displaced vertices,” *Phys. Rev. D* **89**, 073005 (2014) Erratum: [*Phys. Rev. D* **93**, no. 9, 099902 (2016)] [arXiv:1312.2900 [hep-ph]], G. Cottin, J. C. Helo and M. Hirsch, “Searches for light sterile neutrinos with multitrack displaced vertices,” *Phys. Rev. D* **97**, no. 5, 055025 (2018) [arXiv:1801.02734 [hep-ph]], G. Cottin, J. C. Helo and M. Hirsch, “Displaced vertices as probes of sterile neutrino mixing at the LHC,” *Phys. Rev. D* **98**, no. 3, 035012 (2018) [arXiv:1806.05191 [hep-ph]], D. Curtin *et al.*, “Long-Lived Particles at the Energy Frontier: The MATHUSLA Physics Case,” arXiv:1806.07396 [hep-ph], D. Dercks, H. K. Dreiner, M. Hirsch and Z. S. Wang, “Long-Lived Fermions at AL3X,” *Phys. Rev. D* **99**, no. 5, 055020 (2019) [arXiv:1811.01995 [hep-ph]], G. Cottin, J. C. Helo, M. Hirsch and D. Silva, “Revisiting the LHC reach in the displaced region of the minimal left-right symmetric model,” arXiv:1902.05673 [hep-ph], C. W. Chiang, G. Cottin, A. Das and S. Mandal, “Displaced heavy neutrinos from  $Z'$  decays at the LHC,” arXiv:1908.09838 [hep-ph], C. Arbez, J. C. Helo and M. Hirsch, “Long-lived heavy particles in neutrino mass models,” *Phys. Rev. D* **100**, no. 5, 055001 (2019) [arXiv:1906.03030 [hep-ph]]. A. Das, P. S. B. Dev and N. Okada, “Long-lived TeV-scale right-handed neutrino production at the LHC in gauged  $U(1)_X$  model,” *Phys. Lett. B* **799**, 135052 (2019) [arXiv:1906.04132 [hep-ph]].
- [36] P. S. Bhupal Dev and Y. Zhang, “Displaced vertex signatures of doubly charged scalars in the type-II seesaw and its left-right extensions,” *JHEP* **1810**, 199 (2018) [arXiv:1808.00943 [hep-ph]].
- [37] M. Cirelli, N. Fornengo and A. Strumia, “Minimal dark matter,” *Nucl. Phys. B* **753**, 178 (2006) [hep-ph/0512090].
- [38] F. P. An *et al.* [Daya Bay Collaboration], “Observation of electron-antineutrino disappearance at Daya Bay,” *Phys. Rev. Lett.* **108**, 171803 (2012) [arXiv:1203.1669 [hep-ex]].
- [39] J. Heeck, “Unbroken  $B-L$  symmetry,” *Phys. Lett. B* **739**, 256 (2014) [arXiv:1408.6845 [hep-ph]].
- [40] M. Tanabashi *et al.* [Particle Data Group], “Review of Particle Physics,” *Phys. Rev. D* **98**, no. 3, 030001 (2018).

- [41] J. A. Casas and A. Ibarra, “Oscillating neutrinos and muon  $\rightarrow e, \gamma$ ,” Nucl. Phys. B **618**, 171 (2001) [hep-ph/0103065].
- [42] J. Alwall, M. Herquet, F. Maltoni, O. Mattelaer and T. Stelzer, “MadGraph 5 : Going Beyond,” JHEP **1106**, 128 (2011) [arXiv:1106.0522 [hep-ph]].
- [43] J. Alwall *et al.*, “The automated computation of tree-level and next-to-leading order differential cross sections, and their matching to parton shower simulations,” JHEP **1407**, 079 (2014) [arXiv:1405.0301 [hep-ph]].
- [44] R. Franceschini, T. Hambye and A. Strumia, “Type-III see-saw at LHC,” Phys. Rev. D **78**, 033002 (2008) [arXiv:0805.1613 [hep-ph]].
- [45] R. Mahbubani, P. Schwaller and J. Zurita, “Closing the window for compressed Dark Sectors with disappearing charged tracks,” JHEP **1706**, 119 (2017) Erratum: [JHEP **1710**, 061 (2017)] [arXiv:1703.05327 [hep-ph]].
- [46] D. Curtin and M. E. Peskin, “Analysis of Long Lived Particle Decays with the MATH-USLA Detector,” Phys. Rev. D **97**, no. 1, 015006 (2018) [arXiv:1705.06327 [hep-ph]].
- [47] D. Curtin, K. Deshpande, O. Fischer and J. Zurita, “New Physics Opportunities for Long-Lived Particles at Electron-Proton Colliders,” JHEP **1807**, 024 (2018) [arXiv:1712.07135 [hep-ph]].